Available online at www.sciencedirect.com

SciVerse ScienceDirect

Ceramics International 38 (2012) 6295–6301

CERAMICS INTERNATIONAL

www.elsevier.com/locate/ceramint

# Effect of indium concentration on morphology and optical properties of In-doped ZnO nanostructures

Ramin Yousefi[a,*], Farid Jamali-Sheini[b], A. Khorsand Zak[c], M.R. Mahmoudian[d]

[a]Department of Physics, Masjed-Soleiman Branch, Islamic Azad University (I.A.U), Masjed-Soleiman, Iran
[b]Department of Physics, Ahwaz Branch, Islamic Azad University, Ahwaz, Iran
[c]Materials and Electroceramics Lab., Department of Physics, Faculty of Science, Ferdowsi University of Mashhad, Iran
[d]Department of Chemistry, University of Malaya, Kuala Lumpur 50603, Malaysia

Received 16 April 2012; received in revised form 29 April 2012; accepted 29 April 2012
Available online 9 May 2012

**Abstract**

In-doped ZnO nanostructures with different indium concentrations were grown using a thermal evaporation method. The In-doped ZnO nanostructures with a low concentration of indium exhibited a javelin shape, while the In-doped ZnO nanostructures with a high concentration of indium showed a flake shape. In addition, undoped ZnO nanojavelins were grown under the same conditions, but the sizes of these undoped ZnO nanojavelins were larger than the In-doped ZnO nanojavelins. It was shown that the $In^{3+}$ cations played a crucial role in controlling the size. X-ray diffraction and Raman spectroscopy clearly showed hexagonal structures for all of the products. However, the Raman results demonstrated that the In-doped ZnO nanoflakes had a lower crystalline quality than the In-doped ZnO nanojavelins. Furthermore, photoluminescence (PL) measurements confirmed the Raman results. Moreover, the PL results demonstrated a larger band-gap for the In-doped ZnO nanostructures in comparison to the undoped ZnO.


*Keywords:* In-doped ZnO nanojavelins; In-doped ZnO nanoflakes; Auger electrons; Optical properties

## 1. Introduction

Zinc oxide (ZnO) is an n-type metal oxide semiconductor with a wide band-gap (3.36 eV) and large excitation binding energy. These characteristics make this material interesting for many applications such as solar cells [1] and field emission applications [2]. The role of the nanostructure size, doping, impurities, and morphology is very important to these applications, which has driven researchers to focus on the synthesis of doped and undoped nanocrystalline ZnO in recent years. Several studies have recently been carried out to investigate the properties of ZnO nanostructures with various shapes [3–7]. In addition, the doping of semiconductors with various elements is known to greatly affect many of the basic physical properties of the semiconductor, including its electrical, optical, and magnetic properties, which are all crucial for most practical applications. In addition to ours, many groups have reported the synthesis of doped ZnO nanostructures with various shapes using different methods [8–11]. Typically, group III (Al, Ga, and In) elements are used to dope ZnO with donor impurities. Accordingly, many studies have already been performed on the synthesis and characterization of doped ZnO nanostructures with these elements [12,13]. However, In-doped ZnO nanostructures are reported several times more often than the use of other group III elements as dopant materials in ZnO nanostructures. Because indium doping is important in the semiconductor industry, many research groups focus on the development of In-doped ZnO nanostructures [14,15]. In-doped ZnO films show similar electrical conductivity and better transparency in both the visible and IR regions compared to indium tin oxide (ITO). Thus, they can be widely used as transparent conductors in many applications [16]. Furthermore, indium is one of the best elements for the band-gap engineering of ZnO, provided that the content is carefully controlled [17–26]. We also investigated the self-catalytic role of indium oxide in the growth process of ZnO/ZnInO heterostructure nanowires that

*Corresponding author. Tel.: +989166224993; fax: +986813330093.
*E-mail address:* yousefi.ramin@gmail.com (R. Yousefi).

0272-8842/$36.00 
http://dx.doi.org/10.1016/j.ceramint.2012.04.085

were grown on a Si(111) substrate using a thermal evaporation setup and studied the effect of indium on the optical properties of the products [27]. We applied a sintering method to prepare the source material to obtain a mix phase of ZnO–$In_2O_3$ and then used it to grow ZnO nanostructures in a tube furnace setup.

In this work, to complete our knowledge of the effect of indium on the morphology and optical properties of ZnO nanostructures, we changed the previous experimental conditions (ZnO and $In_2O_3$ powders were separated in the tube furnace) to obtain ZnO nanostructures with different morphologies. Under the new conditions, undoped ZnO and In-doped ZnO nanostructures with javelin shapes were obtained. In addition, by increasing the indium concentration in the tube furnace, ZnO nanostructures with a flake shape were also obtained. The effects of the indium content on the morphology and optical properties of the ZnO nanostructures were investigated using several tools.

## 2. Experimental

The growth of In-doped ZnO nanostructures was performed in a horizontal tube furnace. The details of the setup were described elsewhere [4] First, Si(111) substrates were ultrasonically cleaned using ethanol and de-ionized water. They were then lightly etched with an HF (43%) and de-ionized water mixture (1:10) for about 10 min to remove the native oxide layer. A mixture of zinc oxide powder (99.99%) and commercial graphite powder at a 1:1 weight ratio was used as the precursor material for the ZnO, and $In_2O_3$ powder (99.99%) was used for the In precursor material ($Mol_{ZnO}/Mol_{In_2O_3} = 10:2$ and $10:3$). The precursor material for the ZnO was placed at the closed end of a small quartz tube, while the $In_2O_3$ powder was placed 10 cm away from the ZnO material, and a Si(111) substrate was placed downstream of the precursor materials, as shown in Fig. 1. The small tube was then inserted into the vacuum chamber so that the closed end was at the center of the furnace. The ZnO and $In_2O_3$ precursor materials were heated to 950 and 850 °C, respectively, and the temperature of the substrate was maintained at 600 °C during the growth process for the In-doped ZnO nanostructures (Fig. 1). High purity $N_2$ gas was fed at about 100 sccm into the furnace at one end, while the other end was connected to a rotary pump. The growth process was allowed to proceed for 1 h. A vacuum of 6 Torr was maintained inside the tube furnace during the deposition of the nanostructures. In this manner, three sets of In-doped ZnO nanostructures made with different indium content. Undoped ZnO nanostructures were also grown under the same conditions using a catalyst-free substrate. The crystal structure and morphology of the products were investigated using a field emission scanning electron microscope (FESEM, Quanta 200F) and an x-ray diffractometer (XRD, Siemens D5000). The elemental contents of the products were measured using energy dispersive x-ray (EDX, Quanta 200F) and field emission Auger electron spectrometers (FEAES, Jamp-9500F). A room temperature photoluminescence (PL) spectrometer and Raman (Jobin Yvon Horiba HR 800 UV) measurements were employed to study the optical properties and crystallinity of the In-doped ZnO nanostructures and undoped ZnO javelins. A He–Cd laser with a wavelength of 325 nm and an Ar ion laser with an emission wavelength of 514.5 nm were used for the PL and Raman measurements, respectively.

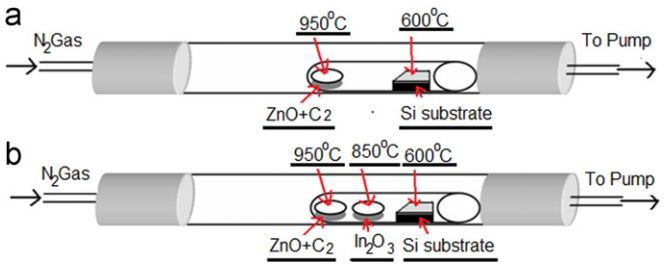


Fig. 1. (a) Schematic of set-up used for growth of undoped ZnO nanostructures. (b) Schematic of set-up used for growth of In-doped ZnO nanostructures.

## 3. Results and discussion

Fig. 2 shows XRD patterns of the undoped ZnO and In-doped ZnO nanostructures. The XRD patterns in Fig. 2 agree with the standard card for bulk ZnO with a hexagonal structure (JCPDS No. 800075). No peaks from Zn, In, or other impurities are visible. The full width at half maximum (FWHM) of all the peaks in the In-doped ZnO nanostructure patterns are wider than those of the undoped ZnO. This may be due to a result of the different sizes or because of the use of indium as an impurity in the In-doped ZnO nanostructures. Thus, doping with indium causes a widening in the peaks [8]. In addition, the wider peaks in the XRD pattern of the In-doped ZnO nanostructures with larger indium content could be a sign that, this sample has a lower crystalline quality than the other

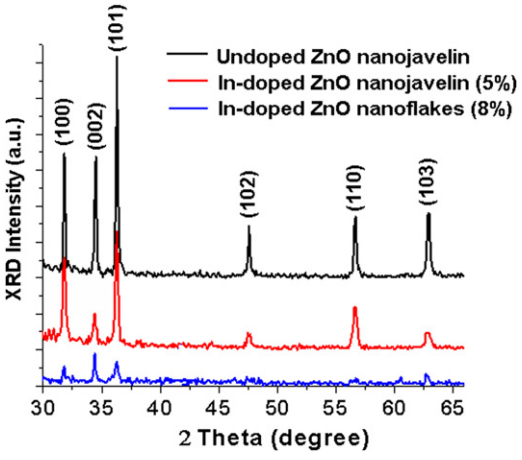


Fig. 2. XRD patterns of undoped ZnO and In-doped ZnO nanostructures. The XRD pattern of undoped ZnO nanostructures shows sharper peaks than the peaks of the XRD patterns of In-doped ZnO nanostructures.

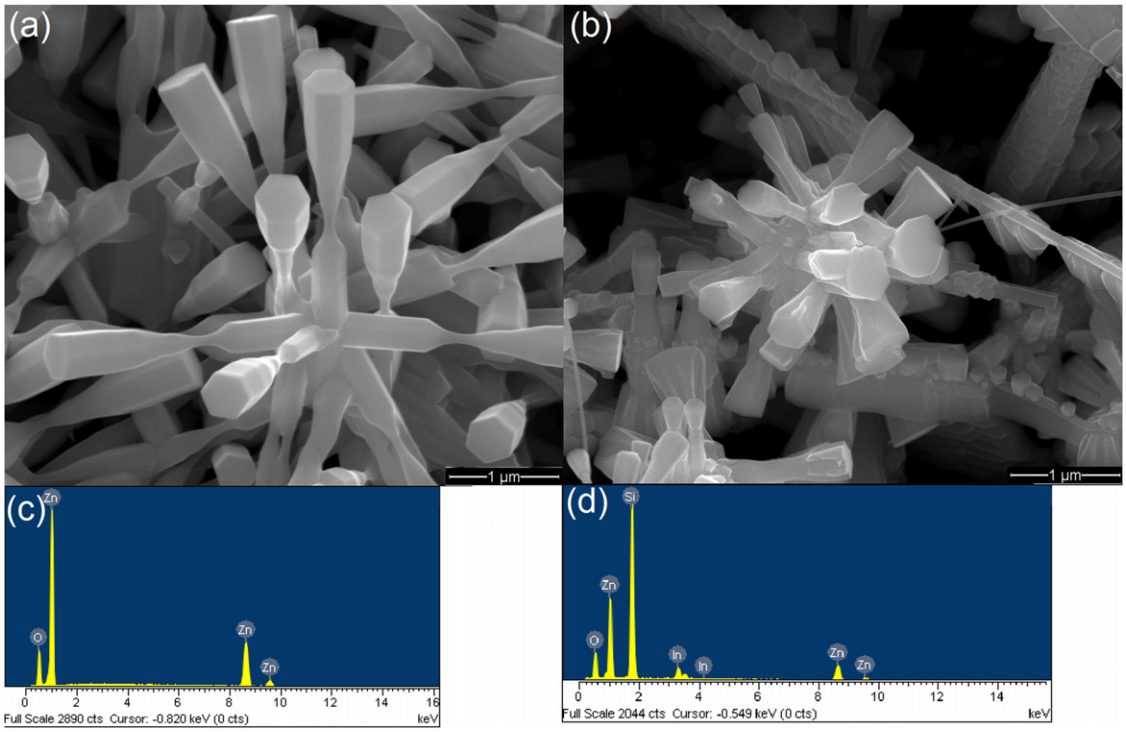


Fig. 3. (a) FESEM image of the undoped ZnO nanojavelins. (b) FESEM image of the In-doped ZnO nanojavelins. (c) EDX spectrum of the undoped ZnO nanojavelins. (d) EDX spectrum of the In-doped ZnO nanojavelins.

samples. These results provide indirect evidence that indium was incorporated into the crystal structure of ZnO.

Fig. 3(a) shows an FESEM image of the undoped ZnO nanostructures. It can be clearly seen that the morphology of the nanostructures is javelin-shaped. As can be seen, these javelins have a perfect hexagonal geometry. The average diameter of the javelins is about 350 nm at the tip, and the average base diameter of is 100 nm, with several micrometers in length. The orientation of the javelins growth is preferentially along the direction of the *c*-axis ([0001]), because the *c*-axis is perpendicular to the hexagonal plane. Fig. 3(b) shows an FESEM image of the In-doped ZnO nanostructures. The morphology of In-doped ZnO nanostructures is also javelin-shape. However, the average diameter at the tip of the In-doped ZnO nanojavelins is smaller (150 nm) than the average diameter of the undoped ZnO nanojavelins. In addition, the lengths of the In-doped ZnO nanojavelins are approximately a few micrometers. As can be observed from their hexagonal tips, the In-doped ZnO nanojavelins were also grown along in the *c*-direction. Fig. 3(c) and (d) show EDX spectra of the undoped and In-doped ZnO nanojavelins, respectively. The EDX spectrum of the In-doped ZnO nanojavelins shows about a 5% (atomic) content for the In element and no peaks are detected from other materials (Fig. 3(d)), while the EDX spectrum in Fig. 3(c) shows that the undoped ZnO nanojavelins are pure ZnO.

To understand the effect of indium on the growth process of the In-doped ZnO nanostructures, In-doped ZnO nanostructures with a higher concentration of indium were examined under the same conditions described above. Fig. 4 shows an FESEM image and the EDX spectrum of a top view of In-doped ZnO nanostructures that were grown with a higher indium concentration. Compared to the In-doped ZnO nanojavelins, these nanostructures show a stacked nanoflake shape. A carefully microscopy study helped us to obtain the several nanoflakes with hexagonal shapes that can be seen in Fig. 4(b). Furthermore, the EDX spectrum from the top view (Fig. 4(c)) reveals a higher concentration of indium than was observed previously (8% atomic).

Field emission Auger electron spectroscopy (FEAES) supports the EDX results. Fig. 5(a)–(c) show high resolution N (E) Auger electron spectroscopy of indium, oxygen, and zinc, respectively, for a single In-doped ZnO nanojavelin, nanoflake and undoped ZnO nanojavelin. As illustrated in Fig. 5(a), an indium peak at 395 eV is evident for the In-doped ZnO nanostructures. This corresponds to MNN Auger electron emission from the indium. In contrast, no peak associated with indium is observed in the undoped ZnO nanojavelin. The FEAES spectra of oxygen (Fig. 5(b)) indicate clear peaks at 487 and 505 eV for the In-doped ZnO nanostructures, while these peaks lie at 480 and 501 eV for the undoped ZnO nanojavelin. These correspond to KLL Auger electron emissions from oxygen. Finally, the FEAES spectra for zinc, as shown in Fig. 5(c), have peaks at 898, 984, and 1006 eV for the In-doped of the single nanojavelin and nanoflake, while these appear at 891, 982, and 1004 eV for the undoped ZnO nanojavelin. These correspond to LMM Auger electron emission from

zinc. We also observed such shifts in energy of Auger electrons in our previous study of In-doped ZnO nanowires [27]. We proposed that such shifts could show the incorporation of indium into the crystal structure of ZnO.

$$\mathrm{O(KLL)}\begin{cases}480\ \mathrm{eV\ (undoped\ ZnO)}\rightarrow 487\ \mathrm{eV\ (In\text{-}doped)}\\ 501\ \mathrm{eV\ (undoped\ ZnO)}\rightarrow 505\ \mathrm{eV\ (In\text{-}doped\ ZnO)}\end{cases} \quad (1)$$

$$\mathrm{Zn(LMM)}\begin{cases}982\ \mathrm{eV\ (undoped\ \ ZnO)}\rightarrow 984\ \mathrm{eV\ (In\text{-}doped\ ZnO)}\\ 891\ \mathrm{eV\ (undoped\ \ ZnO)}\rightarrow 898\ \mathrm{eV\ (In\text{-}doped\ ZnO)}\\ 1004\ \mathrm{eV\ (undoped\ \ ZnO)}\rightarrow 1006\ \mathrm{eV\ (In\text{-}doped\ ZnO)}\end{cases}$$

It is known that diffusion will occur even if the total pressure is constant and uniform inside the tube, as long as there is a spatial difference in the chemical potential. Such a potential is normally represented by the difference in the concentrations or partial pressures of the compounds in a gas mixture. Because of this, the corresponding vapors could propagate toward the substrate in our configuration. In addition, because no catalyst was used in the growth of the products in this study, the vapor-liquid-solid (VLS) mechanism could not be responsible for the growth; in fact, the growth occurred via a vapor–solid (VS) mechanism. The absence of any detectable catalyst and impurity at the ZnO nanostructure surface supports this statement. Therefore, the growth process for the undoped ZnO nanojavelin can be explained by the following reactions:

$$\mathrm{ZnO(s)+C(s)\rightarrow Zn(g)+CO(g)} \quad (2)$$

$$\mathrm{ZnO(s)+CO(g)\rightarrow Zn(g)+CO_2(g)} \quad (3)$$

$$\mathrm{Zn(g)+CO(g)\rightarrow ZnO(nanojavelins)+C(s)} \quad (4)$$

In fact, graphite was introduced into the raw materials to reduce the oxides in the metals, as shown in reaction (2). Moreover, the sublimed Zn atoms are carried downstream by the diffusion process, and in the lower-temperature region, Zn atoms condense and form liquid clusters, which tend to deposit fairly uniformly onto the silicon substrate. The liquid droplets quickly solidify on the substrate in the deposition temperature zone. From a surface-energy point of view, the lowest energy facets for Zn are {0001}, and then $\{10\bar{1}0\}$ and $\{2\bar{1}\bar{1}0\}$. Thus, faceted, single crystalline Zn hexagonal javelins tend to form, which are enclosed by {0001} top and bottom surfaces and $\{10\bar{1}0\}$ side surfaces. Considering the lower local growth temperature, the residual oxygen in the growth chamber is likely to oxidize the surface of the Zn javelins, but the degree of oxidation in the javelins depends on the local temperature and amount of oxygen in chamber. Based on the information that we gathered, a growth process for the hexagonal In-doped ZnO nanojavelins and nanoflakes can be proposed. If the (0002) facet of the crystallized ZnO is constantly kept clean and the newly incoming droplets can constantly wet and cover the entire condensed (0002) facet, the ZnO nanojavelins with a geometrical shape

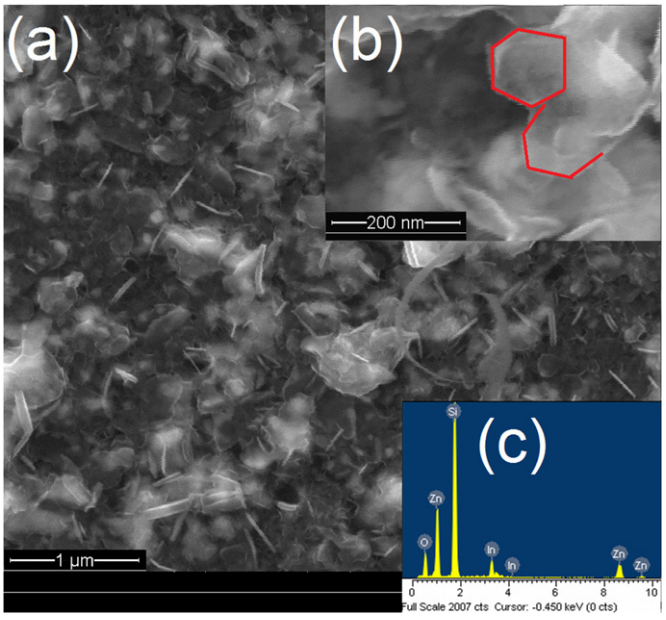


Fig. 4. (a) FESEM image of the In-doped ZnO nanoflakes. (b) High magnification of some nanoflakes with a hexagonal shape. (c) EDX spectrum of the In-doped ZnO nanoflakes.

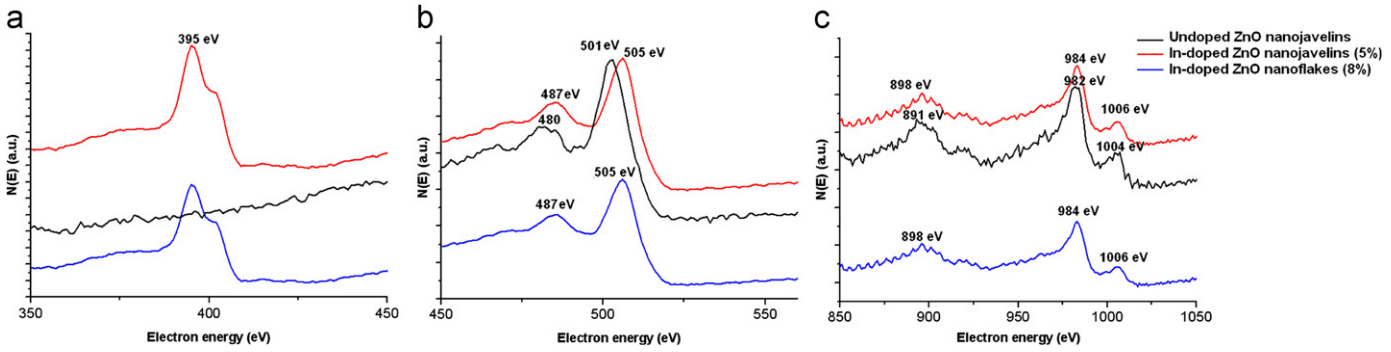


Fig. 5. High-resolution N (E) Auger electron emission spectroscopy of the undoped ZnO nanojavelin, In-doped ZnO nanojavelin, and In-doped ZnO nanoflake. (a) Indium spectra corresponding to the MNN Auger electron emission from indium (In (MNN)). These spectra show that the indium element is only detectable in the In-doped ZnO nanostructures. (b) Oxygen spectra corresponding to the KLL Auger electron emission from oxygen (O (KLL)). (c) Zinc spectra corresponding to the LMM Auger electron emission from zinc (Zn (LMM)). Spectra of oxygen and zinc clearly show a slight shift towards higher energies for the In-doped ZnO nanostructures compared with the undoped ZnO nanostructures.

consisting of hexagonal projections can be obtained [28]. Under our experimental conditions, the mobility of the Zn atoms in the vapor was high enough to form flat (0002) surfaces which prevented the accumulation of incoming atoms or molecules [29] The smooth surface of the javelins, as shown in the SEM image in Fig. 2(a), provides the evidence for this assumption. However, one question arises here: Why were nanostructures with smaller sizes obtained from the samples that were doped with In? According to the following reactions.

$$In_2O_3(g)+3CO(g)\ (\text{from reaction (2)})\rightarrow 2\,In(g)+3CO_2(g) \quad (5)$$

$$(3-2x)Zn(g)+3xCO(g)+4xIn(g)+(1/2+3x)O_2\rightarrow Zn_{(3-2x)}In_{2x}O(\text{nanostructures})+xIn_2(CO_3)_3 \quad (6)$$

Some of the oxygen in the chamber serves to generate $xIn_2(CO_3)_3$ and indium substitutes for zinc during the oxidation of the Zn. Therefore, the lower oxidation of the Zn droplets during the growth of the In-doped ZnO nanostructures causes the sizes of the In-doped ZnO nanostructures to be smaller than the undoped ZnO. Thus, we infer that the $In^{3+}$ may serve as a surface-passivating agent in the reaction system. Because the ZnO crystal is a polar material in nature with a $(000\bar{1})$ surface terminated by $O^{2-}$ ions, the opposite ions ($In^{3+}$) would be adsorbed by charge compensation. The adsorption of $In^{3+}$ on the $O^{2-}$ terminated faces resulted in the redistribution of the surface energy and the growth rates of the different facets changed. The growth process took place at the interface of the O terminated facets by the combination of $In^{3+}$. Accordingly, the intrinsic growth of ZnO along the [0001] direction is substantially suppressed forming the ZnO nanostructures. Therefore, we believe that $In^{3+}$ ions act as a passivation agent by charge compensation and slow the growth of ZnO along the [0001] direction, leading to the formation of In-doped ZnO hexagonal nanojavelins and nanoflakes. The role of In as the passivation agent during the growth process of ZnO nanostructures has already been reported by several researchers [30–33].

Raman spectroscopy is an effective technique for estimating the crystallinity of materials. According to the group theory, single crystalline ZnO belongs to the $C_{6V}^4$ space group, with two formula units per primitive cell and eight sets of optical phonon modes at the Γ point of the Brillouin zone, classified as $A_1+E_1+2E_2$ modes (Raman active), $2B_1$ modes (Raman silent) and $A_1+E_1$ modes (infrared active). The $E_1$ and $A_1$ modes are two polar modes and are split into the transverse optical (TO) and longitudinal optical (LO) branches. The Raman spectra for the undoped ZnO nanojavelins and In-doped ZnO nanostructures are presented in Fig. 6. As shown in Fig. 6, the Raman spectrum of the undoped ZnO nanojavelins shows sharp, strong, and dominant peaks at 437 $cm^{-1}$, corresponding to the $E_2$(high) mode of the Raman active mode, a characteristic peak for the wurtzite hexagonal phase of ZnO. On the other hand, the Raman spectrum of the

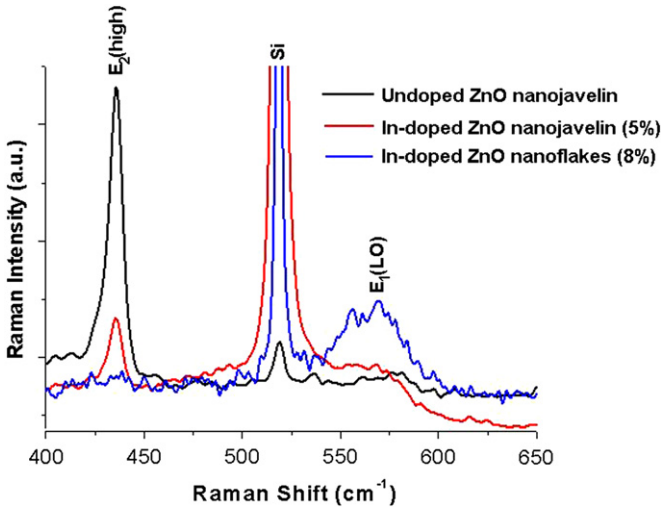


Fig. 6. Raman spectra of the undoped ZnO and In-doped ZnO nanostructures.

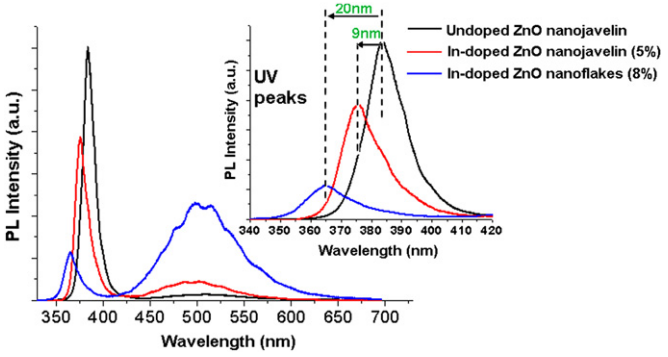


Fig. 7. PL spectra of the undoped ZnO and In-doped ZnO nanostructures.

In-doped ZnO nanojavelins shows a weaker $E_2$(high) peak in comparison to the undoped ZnO nanojavelins and the Raman spectrum of the In-doped ZnO nanoflakes exhibits no detectable $E_2$(high) peak. A strong peak at 579 $cm^{-1}$ corresponding to $E_1$(LO) is indicated for the In-doped ZnO nanoflakes. The $E_1$(LO) mode is associated with impurities and formation defects such as oxygen vacancies [34]. Therefore, the appearance of negligible $E_1$(LO) peaks for the undoped and In-doped ZnO nanojavelins indicates a higher crystalline quality and lower oxygen vacancy for them. On the other hand, the Raman spectrum of In-doped ZnO nanoflakes shows that the crystalline quality of the nanoflakes is lower than that of the other samples. These results are in good agreement with those obtained from the XRD patterns.

A PL study is a powerful method for investigating the effects of doping on the optical properties of ZnO nanostructures, because doped ZnO nanostructures are expected to have different optical properties in comparison to undoped ZnO. Fig. 7 shows the room temperature PL spectra of the undoped ZnO nanojavelins and In-doped ZnO nanostructures. The PL spectrum of the undoped ZnO nanojavelins shows a strong peak in the ultraviolet (UV) region at 382 nm

and a negligible green emission (deep-level emission (DLE)) peaks in the visible region at around 480 nm. In addition, the PL spectrum of the In-doped ZnO nanojavelins indicates a strong UV peak and a weak DLE emission. However, the UV/DLE ratio of the In-doped ZnO nanojavelins, which is one of the main factors that is usually used for comparing the optical properties of samples, is smaller than the UV/DLE ratio of the undoped ZnO nanojavelins. Therefore, the undoped ZnO nanojavelins have a better relative crystalline quality. Furthermore, the PL spectrum of the In-doped ZnO nanoflakes shows a weak UV peak and a strong DLE peak. In fact, with an increase in the indium content of the ZnO structure, the crystalline quality of the ZnO nanostructures decreases. This decrease in the crystallinity of the In-doped ZnO nanostructures can be explained by the formation of band tiling in the band gap, which is often induced by the introduction of impurities into semiconductors. In fact, the PL results confirm the Raman and XRD results. Compared with the undoped ZnO nanojavelins, the PL spectra of the In-doped ZnO nanostructures show an obvious blue shift in the UV emission (the inset of Fig. 7). This blue shift in the UV emission is believed to be a result of the Burstein–Moss effect because of the In doping in the ZnO nanostructures.

## 4. Conclusion

The thermal evaporation method was used to grow undoped ZnO nanojavelins, In-doped ZnO nanojavelins, and nanoflakes. It was suggested that, the $In^{3+}$ played an important role at the $O^{2-}$(0001) surface of the ZnO in the formation of ZnO nanostructures. The FESEM results indicated that increasing the indium content in the ZnO structures could cause a change in the morphology of the nanostructures from a javelin shape to a flake shape. The Raman and PL results showed that the crystalline and optical qualities of the ZnO nanostructures were reduced by In doping. In addition, the UV peaks of the PL spectra were blue-shifted for the doped samples. This indicated that the $In^{3+}$ doping induced the Burestin–Moss effect and band gap widening in the ZnO nanostructures.

## Acknowledgment

R. Yousefi and F. Jamali-Sheini gratefully acknowledge Islamic Azad University, Masjed-Soleiman and Ahwaz Branches, respectively, for their financial supporting in this research work.

## References

[1] A. Qurashi, M.F. Hossain, M. Faiz, N. Tabet, M.W. Alam, N.K. Reddy, Fabrication of well-aligned and dumbbell-shaped hexagonal ZnO nanorod arrays and their dye sensitized solar cell applications, Journal of Alloys and Compounds 503 (2010) L40–L43.

[2] R. Yousefi, F. Jamali-Sheini, M.R. Muhamad, M.A. More, Characterization and field emission properties of ZnMgO nanowires fabricated by thermal evaporation process, Solid State Sciences 12 (2010) 1088.

[3] F. Jamali-Sheini, K.R. Patil, D.S. Joag, M.A. More, Synthesis of Cu–ZnO and C–ZnO nanoneedle arrays on zinc foil by low temperature oxidation route: effect of buffer layers on growth, optical and field emission properties, Applied Surface Science 257 (2011) 8366–8372.

[4] R. Yousefi, A. Khorsand Zak, M.R. Mahmoudian, Growth and characterization of Cl-doped ZnO hexagonal nanodisks, Journal of Solid State Chemistry 184 (2011) 2687.

[5] A. Qurashi, M. Faiz, N. Tabet, M.W. Alam, Low temperature synthesis of hexagonal ZnO nanorods and their hydrogen sensing properties, Superlattices and Microstructures 50 (2011) 173.

[6] A. Qurashi, J.H. Kim, Y.B. Hahn, Etch-free selective area growth of well-aligned ZnO nanorod arrays by economical polymer mask for large-area solar cell applications, Solar Energy Materials and Solar Cells 98 (2012) 476.

[7] R. Yousefi, M.R. Muhamad, A. Khorsand Zak, The effect of source temperature on morphological and optical properties of ZnO nanowires grown using a modified thermal evaporation set-up, Current Applied Physics 11 (2011) 767.

[8] F. Jamali-Sheini, M.A. More, S.R. Jadkar, K.R. Patil, V.K. Pillai, D.S. Joag, Observation of photoconductivity in Sn-doped ZnO nanowires and their photoenhanced field emission behavior, Journal of Physical Chemistry C 114 (2010) 3849.

[9] A. Khorsand Zak, R. Yousefi, W.H. Abd Majid, M.R. Muhamad, Facile synthesis and X-ray peak broadening studies of $Zn_{1-x}Mg_xO$ nanoparticles, Ceramics International 38 (2012) 2059–2064.

[10] R. Yousefi, M.R. Muhamad, Effects of gold catalysts and thermal evaporation method modifications on the growth process of $Zn_{1-x}Mg_xO$ nanowires, Journal of Solid State Chemistry 183 (2010) 1733.

[11] F. Jamali-Sheini, D.S. Joag, M.A. More, Influence of process variables on growth of ZnO nanowires by cathodic electrodeposition on zinc substrate, Thin Solid Films 519 (2010) 184.

[12] S.Y. Bae, C.W. Na, J.H. Kang, J. Park, Comparative structure and optical properties of Ga-, In-, and Sn-doped ZnO nanowires synthesized via thermal evaporation, Journal of Physical Chemistry B 109 (2005) 2526.

[13] C.H. Jung, D.J. Kim, Y.K. Kang, D.H. Yoon, Transparent amorphous In–Ga–Zn–O thin film as function of various gas flows for TFT applications, Thin Solid Films 517 (2009) 4078.

[14] E. Pál, V. Hornok, A. Oszkoó, I. Dékány, Hydrothermal synthesis of prism-like and flower-like ZnO and indium-doped ZnO structures, Colloids and Surfaces A 340 (2009) 1.

[15] M.N. Jung, S.H. Ha, S.J. Oh, J.E. Koo, Y.R. Cho, H.C. Lee, T.I. Jeon, H. Makino, J.H. Chang, Field emission properties of indium-doped ZnO tetrapods, Current Applied Physics 9 (2009) 169.

[16] L.P. Peng, L. Fang, X.F. Yang, Y.J. Li, Q.L. Huang, F. Wu, C.Y. Kong, Effect of annealing temperature on the structure and optical properties of In-doped ZnO thin films, Journal of Alloys and Compounds 484 (2009) 575.

[17] Y. Huang, Y. Zhang, Y. Gu, X. Bai, J. Qi, Q. Liao, J. Liu, Field emission of a single In-doped ZnO nanowire, Journal of Physical Chemistry C 111 (2007) 9039.

[18] L. Xu, Y. Su, Y. Chen, H. Xiao, L. Zhu, Q. Zhou, S. Li, Synthesis and characterization of indium-doped ZnO nanowires with periodical single-twin structures, Journal of Physical Chemistry B, Focus on Physics 110 (2006) 6637.

[19] S.Y. Bae, H.C. Chio, C.W. Na, J. Prk, Influence of in incorporation on the electronic structure of ZnO nanowires, Applied Physics Letters 86 (2005) 033102.

[20] K.J. Kim, Y.R. Park, Large and abrupt optical band gap variation in In-doped ZnO, Applied Physics Letters 78 (2001) 475.

[21] J.Y. Lee, B.R. Jang, J.H. Lee, H.S. Kim, H.K. Cho, J.Y. Moon, H.S. Lee, W.J. Lee, J.W. Baek, Characterization of low mole fraction In-doped-ZnO/Si (111) heterostructure grown by pulsed laser deposition, Thin Solid Films 517 (2009) 4086.

[22] R.K. Gupta, K. Ghosh, R. Patel, S.R. Mishra, P.K. Kahol, Band gap engineering of ZnO thin films by $In_2O_3$ incorporation, Journal of Crystal Growth 310 (2009) 3019.

[23] M.N. Jung, E.S. Lee, T.I. Jeon, K.S. Gil, J.J. Kim, Y. Murakami, S.H. Lee, S.H. Park, H.J. Lee, T. Yao, H. Makino, J.H. Chang, Synthesis and investigation on the extrinsic carrier concentration of indium doped ZnO tetrapods, Journal of Alloys and Compounds 481 (2009) 649.
[24] L.M. Li, C.C. Li, J. Zhang, Z.F. Du, B.S. Zou, H.C. Yu, Y.G. Wang, T.H. Wang, Band gap narrowing and ethanol sensing properties of In-doped ZnO nanowires, Nanotechnology 18 (2007) 225504.
[25] J. Jie, G. Wang, X. Han, J.G. Hou, Synthesis and characterization of aligned ZnO nanorods on porous aluminum oxide template, Journal of Physical Chemistry B 108 (2004) 17027.
[26] J. Jie, G. Wang, X. Han, Q. Yu, Y. Liao, G. Li, J.G. Hou, Indium-doped zinc oxide nanobelts, Chemical Physics Letters 387 (2004) 466.
[27] R. Yousefi, M.R. Muhamad, A.K. Zak, Investigation of indium oxide as a self-catalyst in ZnO/ZnInO heterostructure nanowires growth, Thin Solid Films 518 (2010) 5971.
[28] Z.R. Dai, Z.W. Pan, Z.L. Wang, Novel nanostructures of functional oxides synthesized by thermal evaporation, Advanced Functional Materials 13 (2003) 9.
[29] Z.R. Dai, Z.W. Pan, Z.L. Wang, Gallium oxide nanoribbons and nanosheets, Journal of Physical Chemistry B 106 (2002) 902.
[30] P.F. Lin, C.Y. Ko, W.T. Lin, C.T. Lee, Effects of processing parameters on ultraviolet emission of In-doped ZnO nanodisks grown by carbothermal reduction, Materials Letters 61 (2007) 1767.
[31] N.V. Tuyen, N.N. Long, T.T.Q. Hoa, N.X. Nghia, D.H. Chia, K. Higashimine, T. Mitani, T.D. Canh, Indium-doped zinc oxide nanometer thick disks synthesized by a vapour-phase transport process, Journal of Experimental Nanoscience 4 (2009) 243.
[32] J. Qi, Y. Zhang, Y. Huang, Q. Liao, Juan Liu, Doping and defects in the formation of single-crystal ZnO nanodisks, Applied Physics Letters 89 (2006) 252115.
[33] B. Alemán, P. Fernandez, J. Piqueras, Dense vertical nanoplates arrays and nanobelts of indium doped ZnO grown by thermal treatment of $ZnS–In_2O_3$ powders, Journal of Crystal Growth 312 (2010) 3117–3121.
[34] Y.J. Xing, Z.H. Xi, Z.Q. Xue, X.D. Zhang, J.H. Song, R.M. Wang, J. Xu, Y. Song, S.L. Zhang, D.P. Yu, Optical properties of the ZnO nanotubes synthesized via vapor phase growth, Applied Physics Letters 83 (2003) 1689.